Supplement of Biogeosciences, 17, 6393–6422, 2020
https://doi.org/10.5194/bg-17-6393-2020-supplement

Biogeosciences Open Access EGU

Supplement of

Lagged effects regulate the inter-annual variability of the tropical carbon balance

A. Anthony Bloom et al.

Correspondence to: A. Anthony Bloom (abloom@jpl.nasa.gov)

The following document includes (i) a technical description of the DALEC model version 2a (DALEC2a), (ii) supplementary figures, equations, tables and dataset details ancillary to the primary results presented in the main body of the manuscript.

S1. Description for DALEC2a model and objective function

The equations presented here have been adapted based on the DALEC version presented by Bloom et al. (2016). Advances to the model structure are explicitly discussed in the main body of the manuscript and the corresponding appendices. For a full description of the previous DALEC model versions, we refer the reader to Bloom & William (2015), Williams et al. (2005) and Williams et al. (1997). The DALEC2a parameters and the carbon and water pool symbols are summarized in Table S1. All other terms are explicitly introduced.

S1.1 Carbon pools

$$C_{lab}^{(t+1)} = f_{lab}F_{gpp}^{(t)} + (1 - \phi_{onset}^{(t)})C_{lab}^{(t)}$$

$$C_{fol}^{(t+1)} = \phi_{onset}^{(t)}C_{lab}^{(t)} + (1 - \phi_{fall}^{(t)})C_{fol}^{(t)} + f_{fol}F_{gpp}^{(t)}$$

$$C_{roo}^{(t+1)} = (1 - \theta_{roo})C_{roo}^{(t)} + f_{roo}F_{gpp}^{(t)}$$

$$C_{woo}^{(t+1)} = (1 - \theta_{woo})C_{woo}^{(t)} + f_{woo}F_{gpp}^{(t)}$$

$$C_{lit}^{(t+1)} = \left(1 - (\theta_{lit} + \theta_{\min})\rho^{(t)}\right)C_{lit}^{(t)} + \phi_{fall}^{(t)}C_{fol}^{(t)} + \theta_{roo}C_{roo}^{(t)}$$

$$C_{som}^{(t+1)} = \left(1 - \theta_{som}\,\rho^{(t)}\right)C_{som}^{(t)} + \theta_{woo}\,C_{woo}^{(t)} + \theta_{\min}\rho^{(t)}C_{lit}^{(t)}$$

$F_{gpp}^{(t)}$ is the gross primary production (see S1.2). The time-dependent phenological functions $\phi_{onset}^{(t)}$ and $\phi_{fall}^{(t)}$ are summarized in section S1.3. The formulation of $\rho^{(t)}$ is described in Appendix A2.

S1.2 Fluxes

$$F_{gpp}^{(t)} = F_{gpp(max)}^{(t)} \min\left(\frac{W^{(t)}}{\omega}, 1\right)$$

$$F_{rau}^{(t)} = f_{auto}F_{gpp}^{(t)}$$

$$F_{npp}^{(t)} = F_{gpp}^{(t)} - F_{rau}^{(t)}$$

$$F_{rhe}^{(t)} = \theta_{lit}\rho^{(t)} C_{lit}^{(t)} + \theta_{SOM}\rho^{(t)} C_{SOM}^{(t)}$$

$$F_{nbe}^{(t)} = F_{rhe}^{(t)} + F_{fir}^{(t)} - \mathrm{F}_{npp}^{(\mathrm{t})}$$

The derivation of $F_{gpp(max)}^{(t)}$ is based on the Aggregated Canopy Model (Williams et al., 1997). The specific implementation of ACM in CARDAMOM is described in Bloom et al., (2016) and reference therein. $F_{nbe}^{(t)}$, $F_{rau}^{(t)}$, $F_{rhe}^{(t)}$, $F_{npp}^{(t)}$ and $F_{fir}^{(t)}$ are the net biospheric exchange (NBE), autotrophic respiration (RAU), heterotrophic respiration (RHE), net primary production (NPP) and fire C fluxes respectively. $F_{fir}^{(t)}$ is described in section S1.4.

S1.3 Phenology functions

$$\phi_{onset}^{(t)} = \left(1 - \Phi_{onset}(t, d_{onset}, c_{ronset}, c_{lr})\right)$$

$$\phi_{fall}^{(t)} = \left(1 - \Phi_{fall}\left(t, d_{fall}, c_{fall}, c_{ll}\right)\right)$$

The analytical formulations of Φ_{onset} and Φ_{fall} are described in Bloom & Williams (2015).

S1.4 Fire module

Fire C removals are estimated as

$$C_{lab}^{(t+1)} = C_{lab}^{(t+1)'} - FE_{lab}^{(t)} - FM_{lab}^{(t)}$$

$$C_{fol}^{(t+1)} = C_{fol}^{(t+1)'} - FE_{fol}^{(t)} - FM_{fol}^{(t)}$$

$$C_{roo}^{(t+1)} = C_{roo}^{(t+1)'} - FE_{roo}^{(t)} - FM_{roo}^{(t)}$$

$$C_{woo}^{t+1} = C_{woo}^{t+1\prime} - FE_{woo}^{(t)} - FM_{woo}^{(t)}$$

$$C_{lit}^{t+1} = C_{lit}^{t+1\prime} - FE_{lit}^{(t)} + FM_{lab}^{(t)} + FM_{fol}^{(t)} + FM_{roo}^{(t)}$$

$$C_{som}^{t+1} = C_{som}^{t+1\prime} - FM_{som}^{(t)} + FM_{woo}^{(t)}$$

where FE and FM represent fire emission and fire mortality fluxes, and the "′" denotes the pre-fire estimate of C_i^{t+1} for each pool *i* (see S1.1). Fire emissions for each pool *i* are derived as

$$FE_i^{(t)} = C_i^{(t+1)'} BA_i \, k_{factor(i)}$$

where $k_{factor(i)}$ is the combustion factor for carbon pool *i.* Fire induced mortality rates for each pool *i* are calculated as

$$FM_i^{(t)} = C_i^{(t+1)'} BA_i \left(1 - k_{factor(i)}\right) r$$

In Bloom et al., (2016), k_{factor} values are prescribed; here we summarize the uncertainty of combustion factors as three parameters: π_{foliar}, $\pi_{biomass}$ and π_{soil} (see section 2.1 in the main text). Specifically

$k_{factor(lab,roo,woo)} = \pi_{biomass}$
$k_{foliar(fol)} = \pi_{foliar}$
$k_{factor(lit)} = (\pi_{SOM} + \pi_{foliar})/2$
$k_{factor(som)} = \pi_{SOM}.$

Prior ranges for parameters $\pi_{biomass}$, π_{soil} and *r* are reported in Table S1. As stated in the main text, we appended the ecological and dynamical constraints (EDCs) used by Bloom et al., (2016) to include the following conditions:

$$\pi_{foliar} > \pi_{biomass}$$
$$\pi_{foliar} > \pi_{SOM}$$

S1.5 Plant-available water

The DALEC2a water module is described in Appendix A1 of the main text. For the sake of completes, the equations are re-stated here:

$$W^{(t+1)} = W^{(t)} + (P^{(t)} - ET^{(t)} - R^{(t)})\Delta t$$

$$ET^{(t)} = F_{gpp}^{(t)} \frac{VPD^{(t)}}{\upsilon_e}$$
$$R^{(t)} = aW^{(t)^2}$$

where $W^{(t)}$ is the plant-available water, and $P^{(t)}, ET^{(t)}, R^{(t)}$ are the plant-available water, precipitation, evapotranspiration and runoff water fluxes respectively.

Table S1: Optimized parameters and initial conditions, corresponding prior ranges, and resulting state variables.

	Parameter	Description	Prior range
Allocation fractions	fauto	Autotrophic respiration	0.2 – 0.8
	flab	NPP fraction to labile C	0.01 – 0.5*
	ffol	NPP fraction to foliar C	0.01 – 0.5*
	froo	NPP fraction to fine root C	0.01 – 0.5*
	fwoo[1]	NPP fraction to stem C	0.01 – 0.5*
Turnover rates	θwoo	Stem C turnover rate	2.5×10^{-5} - 10^{-3}
	θroo	Fine root C turnover rate	10^{-4} - 10^{-2}
	θlit	Litter C turnover rate at $\overline{\boldsymbol{T}}$, $\overline{\boldsymbol{P}}$	10^{-4} - 10^{-2}
	θsom	Soil organic matter (SOM) turnover rate at $\overline{\boldsymbol{T}}$, $\overline{\boldsymbol{P}}$	10^{-7} - 10^{-3}
	θmin	Mineralization of litter to SOM at $\overline{\boldsymbol{T}}$, $\overline{\boldsymbol{P}}$	10^{-5} - 10^{-2}
	Θ	Heterotrophic temperature dependence factor	0.018 – 0.08
	s_p	Heterotrophic precipitation dependence factor	0.01 - 1
Canopy parameters	d_{onset}	Leaf onset day	0 – 365.25
	d_{fall}	Leaf fall day	0 – 365.25
	c_{eff}	Canopy efficiency	5 – 50
	c_{LMA}	Leaf C mass per area	5 – 200 gC/m^2
	c_{ll}	Leaf loss fraction	1/8 - 1
	[2]c_{lr}	Annual labile C release fraction	1/8 - 1
	c_{ronset}	Labile release period	10 – 100 days
	c_{rfall}	Leaf fall period	20 – 150 days
Fire paramet	π_{foliar}	Combustion factors of foliar C	0.01 – 1
	$\pi_{biomass}$	Combustion factors of non-foliar biomass C	0.01 – 1
	π_{SOM}	Combustion factor of soil C	0.01 – 1
	r	Resilience factor	0.01 – 1
Water paramet	ω	Water stress threshold	1 – 10^4 Kg H_2O m^{-2}
	υ_e	Inherent water-use efficiency	10 – 50 hPa gC/kg H_2O
	α	[4]Second order runoff decay constant	3×10^{-7} – 0.03 mm^{-1} day^{-1}
State variables[3]	$C_{lab}^{(t)}$	Labile C at time *t*	1 – 2000 gC/m^{-2}
	$C_{fol}^{(t)}$	Foliar C at time *t*	1 – 2000 gC/m^{-2}
	$C_{roo}^{(t)}$	Fine root C at time *t*	1 – 2000 gC/m^{-2}
	$C_{woo}^{(t)}$	Above- and below-ground woody C at time *t*	1 – 10^5 gC/m^{-2}
	$C_{lit}^{(t)}$	Litter C at time *t*	1 – 2000 gC/m^{-2}
	$C_{som}^{(t)}$	Soil organic C at time *t*	1 – 2×10^5 gC/m^{-2}
	$W^{(t)}$	Plant-available water at time *t*	1 – 10^4 mm

[1]f_{woo} is equivalent to $1 - f_{auto} - f_{fol} - f_{lab}$

[2]Labile release fraction was previously set to 1.

[3]Only initial conditions (at time t=0) are optimized in DALEC2a.

*Prior ranges are conservative approximations, see Fox et al., (2009) for details on sequential allocation fraction sampling in DALEC models.

S2. CARDAMOM IAV evaluation datasets

GPP:FLUXCOM RS+METEO GPP (Jung et al., 2020) monthly 0.5 datasets ("ALL-MLM", "ALL-METEO") were obtained from http://www.fluxcom.org/. FLUXSAT GPP was obtained from https://avdc.gsfc.nasa.gov/pub/tmp/FluxSatGPP. We confined the evaluation across all GPP estimates to 2007-2015, given that a sparser measurement record was used to estimate pre-2007 FLUXSAT GPP values (Joiner et al., 2018). CARDAMOM, FLUXCOM and FLUXSAT annual GPP timeseries across the six subcontinental regions and pantropical regions were detrended to minimize impact of decadal trends on IAV evaluation.

ET: FLUXCOM RS+METEO LE fluxes (Jung et al., 2019) were obtained from http://www.fluxcom.org/; LE fluxes were multiplied by vegetated area and within each grid cell, and both GPP and LE were scaled by land fraction. LE fluxes were further divided by 2.26 * 1e6 J kg^{-1} to estimate equivalent ET H_2O flux. MODIS ET (Mu et al., 2011) data were obtained from http://files.ntsg.umt.edu/data/NTSG_Products/. Annual CARDAMOM, FLUXCOM and MODIS timeseries across the six subcontinental regions and pantropical regions were detrended to minimize impact of decadal trends on IAV evaluation.

NOAA ESRL atmospheric CO_2 growth rate: annual surface-based CO_2 growth rate estimates were obtained from NOAA/GML website (www.esrl.noaa.gov/gmd/ccgg/trends/). Atmospheric CO_2 growth rate was multiplied by 2.120 PgC/ppm to estimate atmospheric C growth rate. CARDAMOM NBE and NOAA CO_2 growth rate were both linearly detrended for comparison in the main body of the manuscript.

Table S2:IAV comparisons between GPP and IAV

	GPP mean [gC/m^2/yr] IAV [%]			**ET mean [mm/yr] (IAV [%])**			**LAI mean [m^2/m^2] (IAV [%])**	
	CARDAMOM	FLUXCOM	FLUXSAT	CARDAMOM	FLUXCOM	MODIS	CARDAMOM	MODIS
SH South America	1707 (2.2%)	950 (3.2%)	950 (3.2%)	950 (3.2%)	1065 (0.9%)	894 (3.6%)	2.5 (1.8%)	2.5 (1.0 %)
NH South America	2122 (0.8%)	916 (3.3%)	916 (3.3%)	916 (3.3%)	1313 (0.3%)	1319 (1.3%)	3.7 (1.9%)	4.1 (0.7 %)
Southern Africa	1327 (1.9%)	599 (3.5%)	599 (3.5%)	599 (3.5%)	860 (1.1%)	654 (3.7%)	1.5 (1.6%)	1.6 (2.4 %)
Northern SS Africa	918 (2.5%)	559 (4.3%)	559 (4.3%)	559 (4.3%)	888 (0.7%)	556 (6.8%)	1.3 (2.3%)	1.5 (1.3 %)
Australia	418 (7.4%)	246 (5.5%)	246 (5.5%)	246 (5.5%)	478 (5.9%)	269 (13.4%)	0.6 (4.8%)	0.6 (5.2 %)
SE Asia & Indonesia	2503 (1.7%)	1069 (2.1%)	1069 (2.1%)	1069 (2.1%)	1084 (0.4%)	1235 (1.8%)	3.6 (1.6%)	3.8 (0.7 %)
Tropics	1127 (1.2%)	563 (1.3%)	563 (1.3%)	563 (1.3%)	748 (0.5%)	617 (2.1%)	1.6 (1.1%)	1.7 (0.5 %)
Wet tropics	2232 (1.0%)	1055 (1.7%)	1055 (1.7%)	1055 (1.7%)	1201 (0.3%)	1145 (1.3%)	3.4 (1.0%)	3.6 (0.4 %)
Dry tropics	588 (1.7%)	323 (1.1%)	323 (1.1%)	323 (1.1%)	527 (1.1%)	359 (4.1%)	0.7 (1.8%)	0.8 (1.3 %)

Table S2. Correlations between CARDAMOM and independent GPP and ET estimates[1]

	GPP			ET			LAI
	CA vs FC	***CA vs FS***	***FC vs FC***	***CA vs FC***	***CA vs MO***	***FC vs MO***	***CA vs MO***
SH South America	0.42	0.52	0.57	-0.44	-0.08	0.40	-0.1
NH South America	0.37	0.53	0.81*	0.19	0.41	0.09	0.02
Southern Africa	0.70*	0.39	0.58	-0.50	-0.66*	0.79*	-0.39
Northern SS Africa	0.00	0.01	0.63	-0.63*	0.06	0.39	0.18
Australia	0.82*	0.74*	0.92*	-0.32	-0.19	0.94*	0.46
SE Asia & Indonesia	0.22	0.75*	-0.11	-0.14	0.22	-0.27	0.45
Tropics	0.92*	0.69*	0.74*	0.15	0.05	0.71*	-0.07
Wet tropics	0.22	0.47	0.71*	-0.37	0.08	0.39	0.04
Dry tropics	0.83*	0.81*	0.82*	-0.43	-0.46	0.79*	-0.23

[1]**CA = CARDAMOM, FC = FLUXCOM, FS = FLUXSAT, MO = MODIS**

S3. Objective function

As detailed in section 2.4 (eq. 2 in the main body of the manuscript) the objective function is summarized as p(y|O), where

$$p(y|O) \propto p(y)\, p(O|y);$$

p(y) is the prior probability of CARDAMOM parameters (y) and p(O|y) is the likelihood of observations O given y. Individual terms of p(O|y) are described in the main body of the manuscript (eq. 3-9). Individual terms of p(y) consist of:

$$p(y) \sim p(y)_{uniform}\, p(y)_{gaussian}\, p(y)_{EDC}\, p(y)_{range}$$

Details on $p(y)_{uniform}$, $p(y)_{gaussian}$, $p(y)_{EDC}$ and $p(y)_{range}$ are described in Table S4.

Table S4. Summary of objective function components

Term	Objective function	Details
$p(y)_{uniform}$	1 if y values are within intervals in Table S1 (0 otherwise)	Log-uniform distribution for interval p_min to p_max, (i.e. uniform distribution for log(p) between log(p_min) and log(p_max))
$p(y)_{gaussian}$	exp(-0.5*(p – p0)/sigma)	Solely applied to canopy efficiency (mean = 17.5, unc. factor = 1.5), and CUE (mean = 0.5, uncertainty factor 1.2)
$p(y)_{EDC}$	1 if EDC condition is met, 0 otherwise.	See Bloom et al., (2016) and references therein for full list of ecological and dynamic constraints.
$p(y)_{range}$	1 if all states do not exceed state-variable ranges in Table 1, 0 otherwise	
p(O|y)	See equation 3 in main manuscript.	

Table S5. Summary statistics from ranked ΔNBE^{LAG} IAV sampling[1]

	Median ΔNBE^{LAG} [% of NBE IAV], as reported in Table 3.	Ensemble median ΔNBE^{LAG} *IAV [% of NBE IAV]*	Ensemble 2.5th – 97.5th percentile range ΔNBE^{LAG}
SH South America	63%	62%	41 - 91%
NH South America	105%	98%	54 - 119%
Southern Africa	122%	110%	64 - 157%
Northern SS Africa	71%	71%	48 - 110%
Australia	84%	84%	64 - 100%
SE Asia & Indonesia	41%	42%	33 - 69%
Wet Tropics	45%	45%	31 - 64%
Dry Tropics	83%	80%	50 - 138%
Tropics	64%	63%	42 - 93%

[1]Derived by (a) ranking all 4°×5° grid-cell CARDAMOM samples by their corresponding 2001-2015 ΔNBE^{LAG} IAV, and (b) combining CARDAMOM samples by ranking to generate ensemble of regional and pan-tropical ΔNBE^{LAG} IAV estimates.

Supplementary Figures

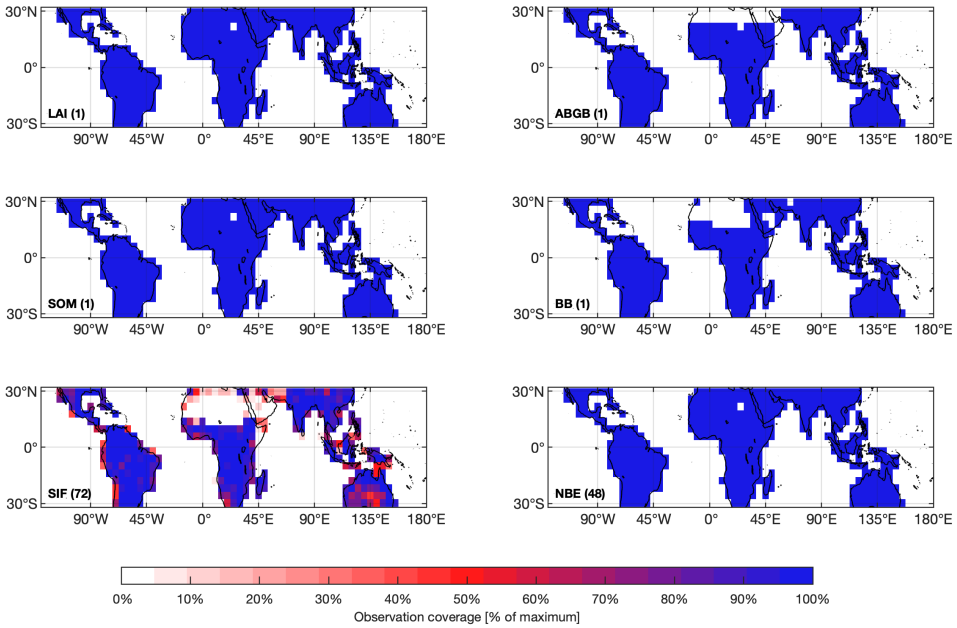

Figure S1: Observational coverage for datasets assimilated in CARDAMOM within each gridcell: the bracketed terms indicate the maximum observations per gridcell across entire study area; colors represent the observational coverage as % of maximum. See Table 1 (main body of the manuscript) for dataset acronym and assimilation details.

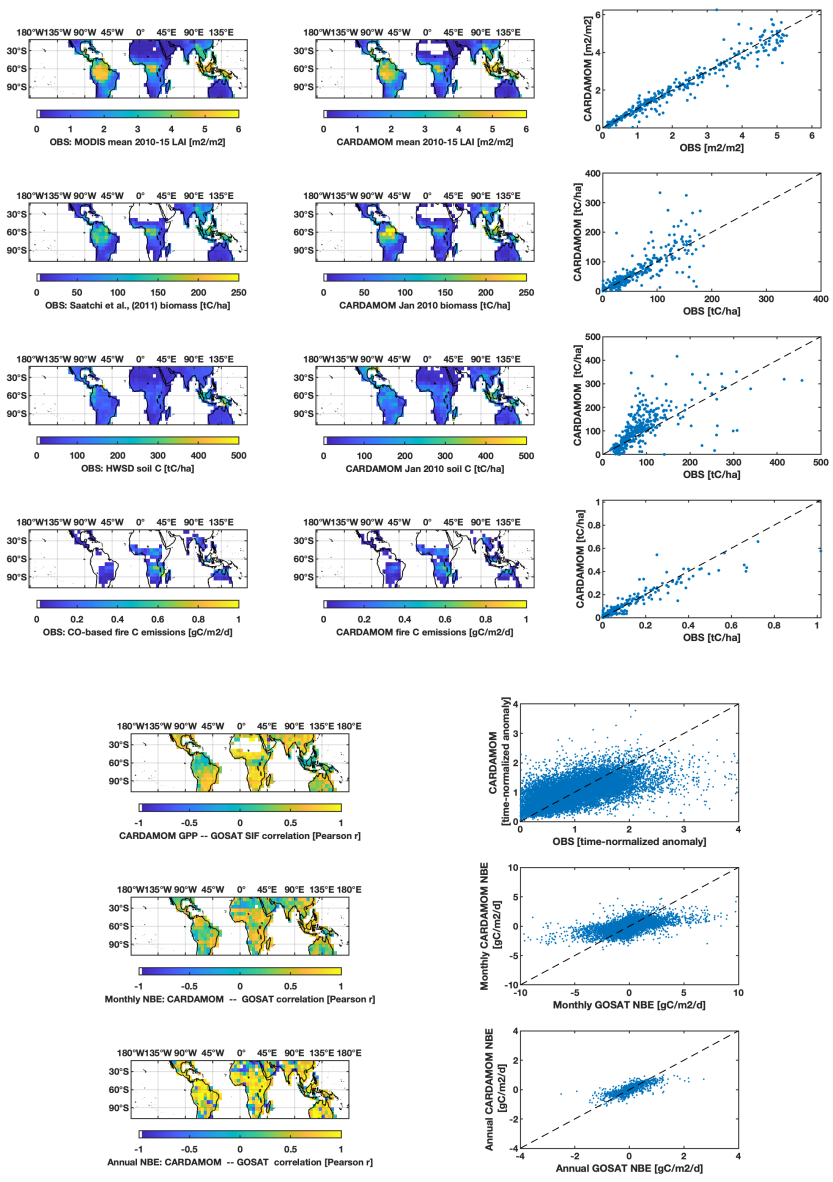

Figure S2: CARDAMOM output comparison against assimilated observational constraints, namely MODIS LAI (top row), Saatchi et al. (2011) biomass (second row), soil carbon from the Harmonized World Soil Database (third row) and fire C emissions as estimated by Worden et al., (2017) (fourth row). CARDAMOM GPP comparison against ingested SIF constraints is summarized in the fifth row: the correlation map denotes the correlation between CARDAMOM GPP and SIF within each grid cell throughout 2010-2015 (fifth row, left panel); comparison between mean-normalized GPP and mean-normalized SIF values across the tropics throughout 2010-2015 (fifth row, right panel). CARDAMOM NBE monthly/annual comparisons against ingested GOSAT-derived NBE constraints are summarized the sixth/seventh rows (respectively): the correlation map denotes the correlation between CARDAMOM and GOSAT-derived NBE within each grid cell throughout 2010-2013 (left panels), and corresponding NBE scatterplots (right panels).

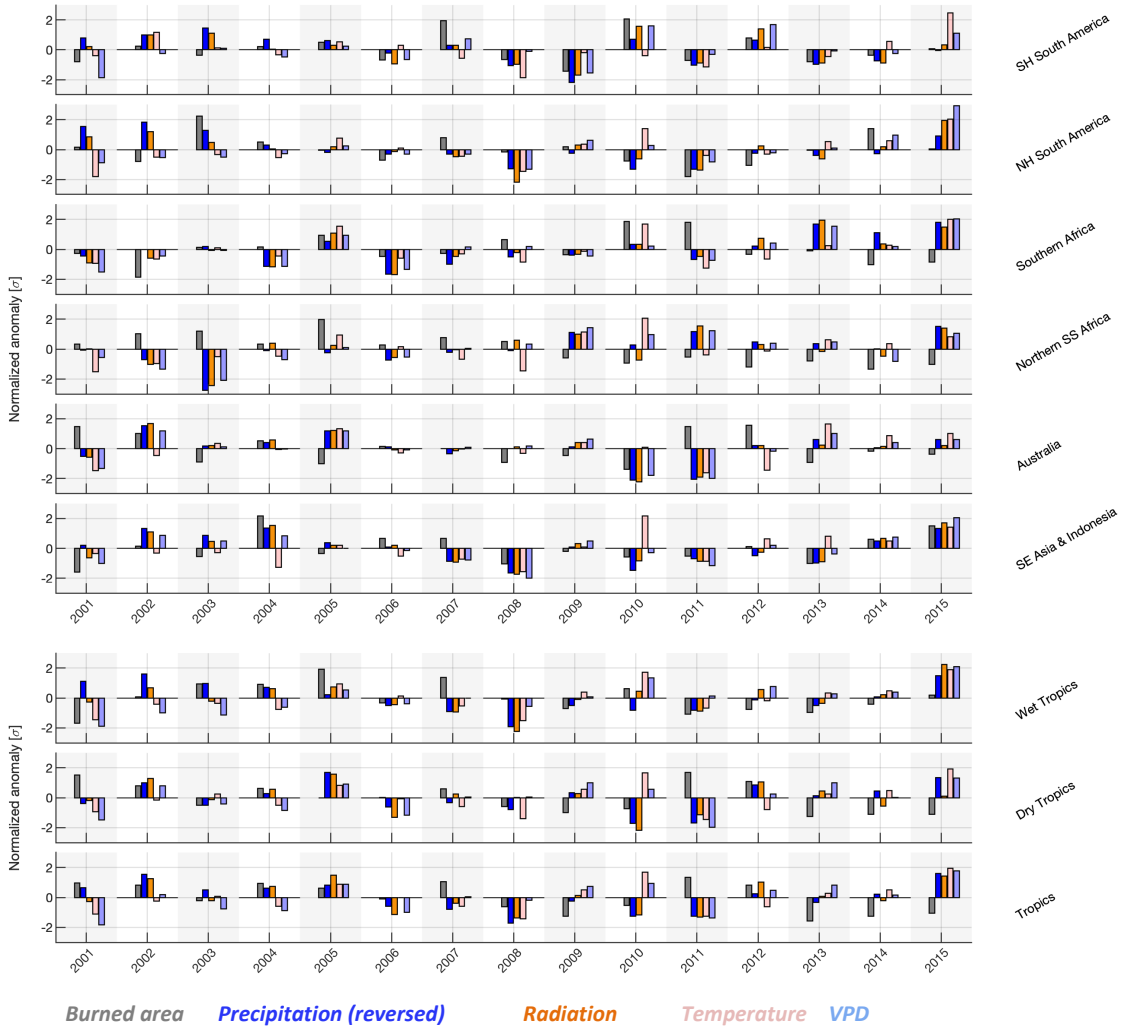

Figure S3. Annual regional and pan-tropical CARDAMOM forcing anomalies throughout 2001-2015; units represent deviations from the mean normalized by the standard deviation. Precipitation anomalies were reversed (i.e. negative values represent positive precipitation anomalies), such that typical dry/warm year forcing conditions correspond to negative deviations for all forcing anomalies (and vice versa). The geographical extent of each region is shown in Figure A1 in the main body of the manuscript.

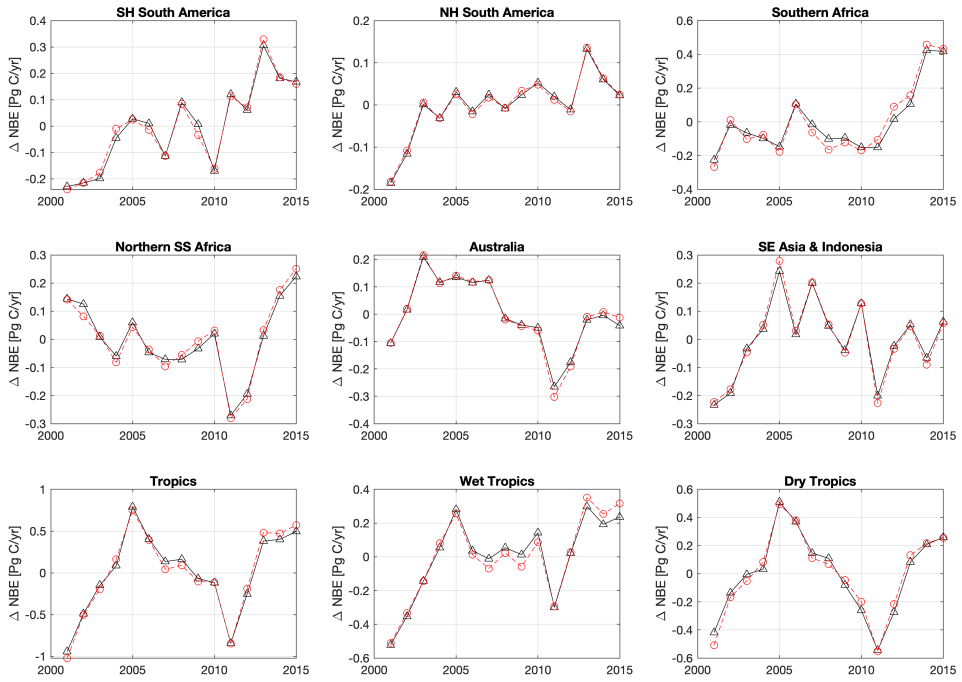

Figure S4: Sum of pool-specific contributions to total NBE lagged effect (red dashed line) and total NBE lagged effects (black solid line) for each region. The geographical extent of each region is shown in Figure A1 in the main body of the manuscript.

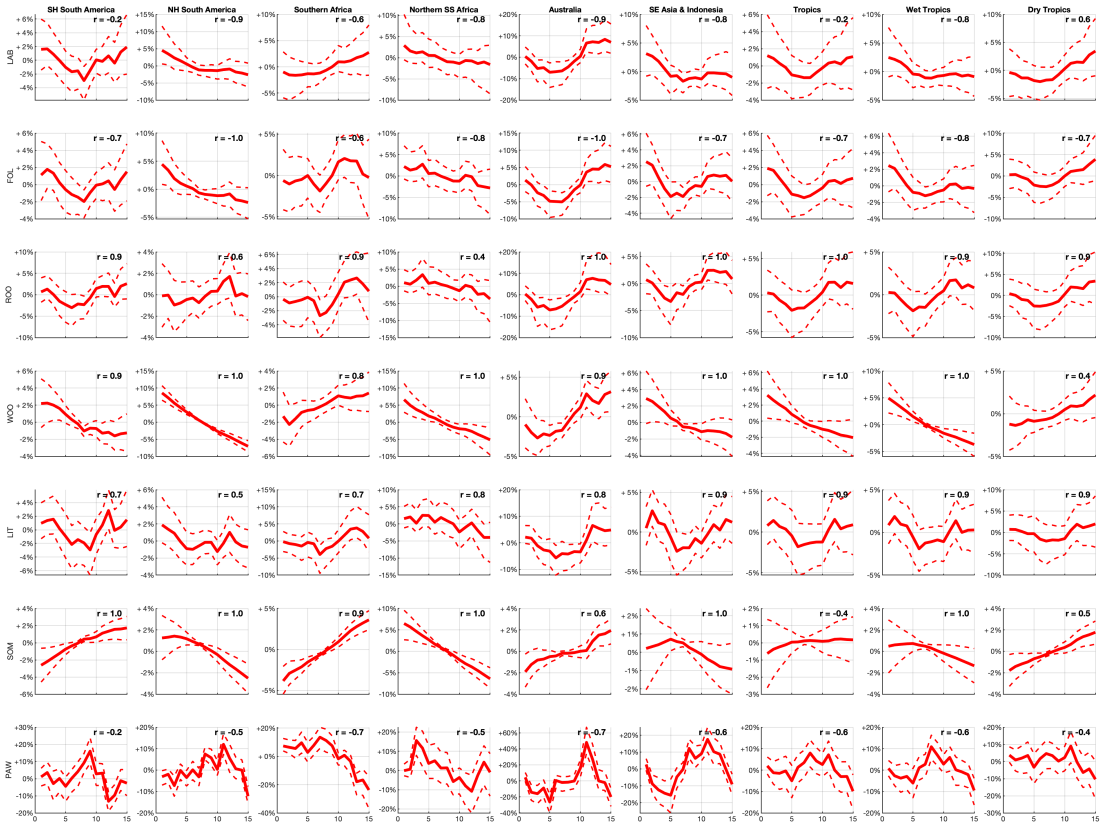

Figure S5: Relative variability of CARDAMOM annual mean carbon and water states throughout 2001-2015 (numbers 1-15 on bottom-row x-axis denote years 2001-2015 respectively); solid/dashed lines represent median and inter-quartile ranges. Pearson r values in top-right corner indicate correlation between relative state variability and pool-specific ΔNBE^{LAG} timeseries (shown in Figure 8).

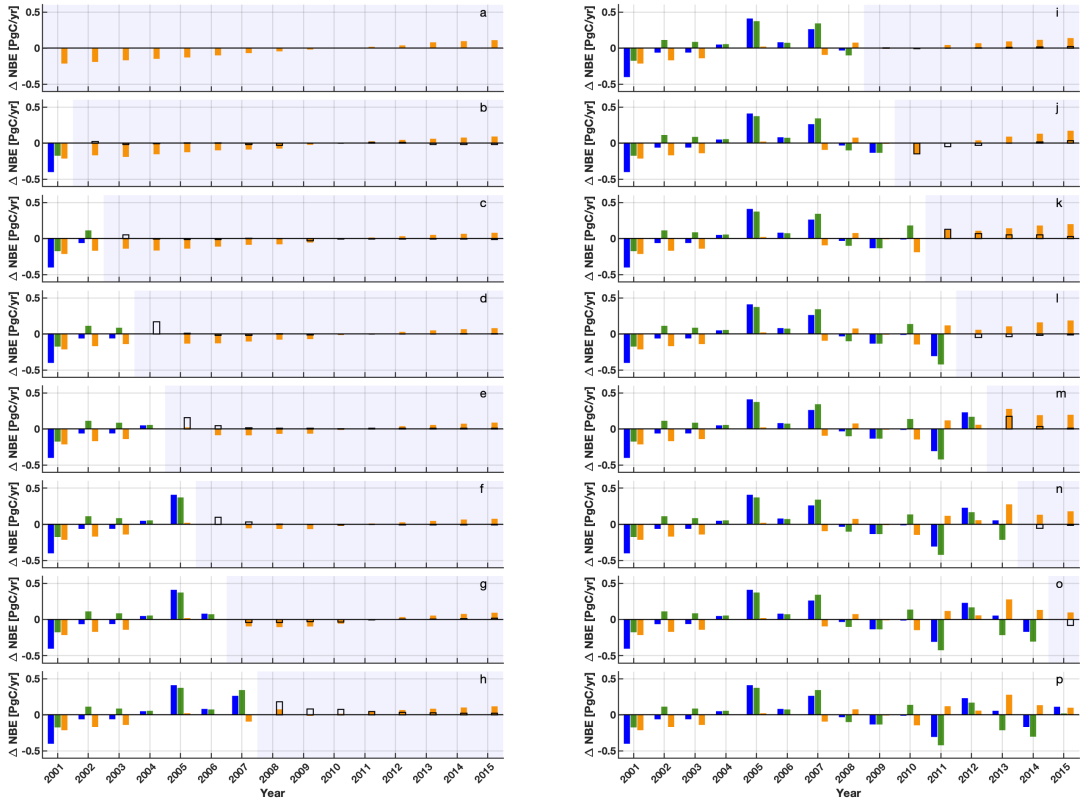

Figure S6: Southern Hemisphere South America 2001-2015 median NBE lagged effect anomalies in the absence of forcing anomaly, i.e. under repeat climatological mean forcing (panel a). Concurrent, total and lagged effects in presence of 2001-onward external forcing (climatological mean forcing + forcing anomaly) and subsequent lagged effects under continued repeat climatological mean forcing (panels b-o); the white background indicates duration of actual forcing, and the blue background indicates duration of repeat climatological mean forcing; the empty bars represent lagged effects attributable to latest annual forcing anomaly under repeat climatological mean forcing. Panel p represents concurrent, lagged and total NBE values; these are equivalent to Figure 6 in the main body of the manuscript.

References

Bloom, A. A. and Williams, M.: Constraining ecosystem carbon dynamics in a data-limited world: integrating ecological "common sense" in a model–data fusion framework, Biogeosciences, 12, 1299–1315, https://doi.org/10.5194/bg-12-1299-2015, 2015.

Bloom, A. A., Exbrayat, J.-F., van der Velde, I. R., Feng, L., and Williams., M.: The decadal state of the terrestrial carbon cycle: Global retrievals of terrestrial carbon allocation, pools, and residence times, P. Natl. Acad. Sci. USA, 113, 1285–1290, https://doi.org/10.1073/pnas.1515160113, 2016.

Fox, A., Williams, M., Richardson, A. D., Cameron, D., Gove, J. H., Quaife, T., Ricciuto, D., Reichstein, M., Tomelleri, E., Trudinger, C. M., and van Wijk, M. T.: The reflex project: com- paring different algorithms and implementations for the inversion of a terrestrial ecosystem model against eddy covariance data, Agr. Forest. Meteorol., 149, 1597–1615, 2009.

Joiner, J., Yoshida, Y., Zhang, Y., Duveiller, G., Jung, M., Lyapustin, A., Wang, Y. and Tucker, C.J.: Estimation of terrestrial global gross primary production (GPP) with satellite data-driven models and eddy covariance flux data. *Remote Sensing*, *10*(9), p.1346, 2018.

Jung, M., Koirala, S., Weber, U., Ichii, K., Gans, F., Camps-Valls, G., Papale, D., Schwalm, C., Tramontana, G. and Reichstein, M.: The FLUXCOM ensemble of global land-atmosphere energy fluxes. Scientific data, 6(1), pp.1-14, 2019.

Jung, M., Schwalm, C., Migliavacca, M., Walther, S., Camps-Valls, G., Koirala, S., Anthoni, P., Besnard, S., Bodesheim, P., Carvalhais, N., Chevallier, F., Gans, F., Goll, D. S., Haverd, V., Köhler, P., Ichii, K., Jain, A. K., Liu, J., Lombardozzi, D., Nabel, J. E. M. S., Nelson, J. A., O'Sullivan, M., Pallandt, M., Papale, D., Peters, W., Pongratz, J., Rödenbeck, C., Sitch, S., Tramontana, G., Walker, A., Weber, U., and Reichstein, M.: Scaling carbon fluxes from eddy covariance sites to globe: synthesis and evaluation of the FLUXCOM approach, Biogeosciences, 17, 1343–1365, https://doi.org/10.5194/bg-17-1343-2020, 2020.

Mu, Q., Zhao, M., & Running, S. W.: Improvements to a MODIS global terrestrial evapotranspiration algorithm. Remote sensing of environment, 115(8), 1781-1800, 2011.

Williams, M., Rastetter, E.B., Fernandes, D.N., Goulden, M.L., Shaver, G.R. and Johnson, L.C.: Predicting gross primary productivity in terrestrial ecosystems. *Ecological Applications*, *7*, 882-894, 1997.

Williams, M., Schwarz, P. A., Law, B. E., Irvine, J., and Kurpius, M. R.: An improved analysis of forest carbon dynamics using data assimilation, Glob. Change Biol., 11, 89–105, 2005.